Electrochemical behavior of titanium-based materials – are there relations to biocompatibility?

D. SCHARNWEBER*, R. BEUTNER, S. RÖßLER, H. WORCH
Dresden University of Technology (TUD), Institute of Materials Science, 01062 Dresden, Germany
E-mail: Dieter.Scharnweber@mailbox.tu-dresden.de

For biomedical applications the physico-chemical properties of oxide layers, always present in titanium-based materials, are of special interest because the biological system is in direct contact only with these oxides. Using electrochemical impedance spectroscopy and galvanostatic polarization it is shown that the different compositions of c.p.-titanium, Ti6Al4V, and Ti6Al7Nb result in different physico-chemical properties of air formed passive layers and anodic oxide layers. This may have a direct impact on the biocompatibility of these materials. Results of impedance spectroscopy distinctly differ in the flatband potentials as well as in the donor densities of air-formed passive layers with Ti6Al7Nb showing an approximately 50% smaller donor density than the other materials. Anodic galvanostatic polarization results in voltage–charge density curves with distinct differences in the Faraday efficiency ε of the oxide formation between Ti6Al7Nb and c.p.-titanium/Ti6Al4V, especially for low current densities. These effects correlate strongly with the donor densities in the air formed passive films of the examined materials.

SEM-images of anodic oxide layers show a blister containing surface morphology of the outer part of the oxide layers for all materials. This morphology is probably caused by oxygen evolution, a process which relies on the transfer of electrons through the growing anodic oxide layers and strongly depends on the donor density in the air formed passive layers. Again, the much more pronounced morphology on c.p. titanium/Ti6Al4V agrees with the different donor densities in the air formed passive layers on the materials.

These findings correlate with the good biocompatibility of Ti6Al7Nb and suggest that conduction mechanisms, in air formed passive layers and anodic oxide layers, contribute to processes that determine the biocompatibility of these materials.

1. Introduction

Titanium-based materials are widely used in modern implantology due to their excellent corrosion behavior and favorable mechanical properties. For the applications as metallic biomaterials the physico-chemical properties (e.g. extent of electronic conductivity) of the oxide layers, always present on these materials, are of special interest because the biological system is in direct contact only with these oxides. It should be expected that the different composition of titanium-based materials results in different physico-chemical properties which may have a direct impact on the biocompatibility of these materials.

Passive layers of a thickness of a few nanometers are formed spontaneously on titanium and titanium-based alloys (on grinded and polished surfaces about 3 nm [1–3]) under atmospheric conditions. According to their physico-chemical behavior these passive layers consist of a substochiometric oxide of the general formula $Ti_{1+x}O_2$, showing n-type semiconductor properties (band gap in dependence on structure between 3.0 and 3.7 eV [4, 5]).

Based on the air-formed passive layers the thickness, composition, structure, and morphology of resulting anodic oxide layers can be varied using electrochemical methods (anodic polarization) in multiple ways. The properties of these oxide layers have to be taken into consideration when applying titanium and titanium-based alloys as metallic biomaterials because they determine decisively the surface chemistry and thus the interactions with biological media including the adsorption of biological molecules.

It should be pointed out here that charge transfer reactions of adsorbed biomolecules – especially proteins – and resulting conformational changes are discussed as a potential reason for immunological reactions caused by implant surfaces – or better by biomolecules with altered conformation due to interactions with these surfaces [6, 7].

It was therefore the goal of this study to compare the

* Author to whom all correspondence should be addressed.

electrochemical and morphological characteristics of air-formed passive films and anodic oxide layers on different widely used titanium-based biomaterials (c.p.-titanium, Ti6Al4V, Ti6Al7Nb). A second aspect was to correlate the structure and properties of the existing air-formed passive layers and newly formed anodic oxide layers with the electrochemical behavior and to draw conclusions for the behavior of these materials as metallic biomaterials.

2. Materials and methods

Discs of c.p.-titanium, Ti6Al4V, and Ti6Al7Nb, with diameters of 10 mm or 16 mm and 2 mm thickness were used as substrates. Surfaces of all materials were prepared by polishing to roughness values below 25 nm (RMS) on a 100 µm length scale. Anodic polarization was performed with a PGZ 301 (Radiometer, Copenhagen, Denmark), EIS measurements with an IM 6 (Zahner Elektrik, Germany) in 0.133 and 0.0133 M phosphate buffer at different pH values. For calculation of impedance parameters the software EQUIVCRT [8] was used. Scanning electron microscopy (SEM) was performed using a DSM 982 Gemini (Carl Zeiss, Oberkochen, Germany) at low acceleration voltage (1 kV) for characterization of morphology.

Focused ion beam (FIB) preparation was performed using a FIB 200 workstation (FEI Company, Hillsboro, Oregon, USA) with a 30 keV Gallium ion beam of a minimum beam diameter of 8 nm. Before FIB preparation, samples were coated with 5 nm Au/Pd (80/20). To obtain sharp cutting edges not influenced by the ion beam, a platinum bar was additionally deposited on the coated surface directly in the FIB-workstation by ion-induced deposition from the gas phase.

3. Results

3.1 Semiconductor-electrochemical properties of air-formed passive layers

For the semiconductor-electrochemical characterization of the air-formed passive layers on the different materials impedance spectra were measured in the potential range between -500 and 1000 mV_{SCE} in 50 mV steps in a frequency range from 1 Hz to 3 kHz. As electrolytes the following phosphate buffers were used to investigate the influence of the pH value of the electrolyte as well as the phosphate concentration: 0.133 M, pH = 4.4, 7.4, and 9.2; 0.0133 M, pH = 7.4.

For analysis of the impedance spectra an equivalent circuit according to Fig. 1 with the ohmic resistance R_Ω of the electrolyte solution in series to a charge transfer resistance R_d and a capacity C in parallel was used similar to literature [7, 9].

From the Mott–Schottky plots of the capacity-values according to the Mott–Schottky–Equation 1

$$\frac{1}{C_{sc}^2} = \frac{2}{q\varepsilon\varepsilon_0 N_d}\left(U - U_{FB} - \frac{kT}{q}\right) \approx \frac{1}{C^2} \qquad (1)$$

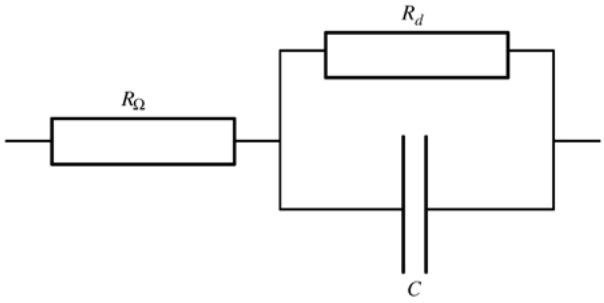

Figure 1 Equivalent circuit used for fitting of data from electrochemical impedance spectroscopy: R_Ω, ohmic resistance of electrolyte solution; R_d, charge transfer resistance; C, capacity (for explanation see Pan *et al*. [9]).

where

C is capacity; C_{SC} is the capacity of space charge layer in the n-type semiconductor; q is the charge of electron (1.602×10^{-19} As); N_d is the donor density (in n-type semiconductor); ε_0 is the absolute dielectric constant (8.86×10^{-14} F cm^{-1}); ε is the relative dielectric constant; U_{FB} is the flatband potential; k is the Boltzmann constant (1.38×10^{-23} Ws K^{-1}; so with $kT/q = 26$ mV important semiconductor properties like the flatband potential U_{FB} and the donor density N_d of the air-formed passive layers present on the materials can be derived as electrochemical parameters [9, 10].

The Mott–Schottky plots of the capacity values in 0.133 M phosphate buffer electrolyte of pH = 7.4 in Fig. 2 show a marked influence of the material composition on the flatband potential which is determined by the intercept of extrapolated lines of the $1/C^2$-plots with the potential axis. Both alloys show more positive flatband potentials than c.p.-titanium whereas Ti6Al7Nb has a flatband potential over 100 mV more negative compared to that of Ti6Al4V. In Fig. 3 the flatband potentials of all materials under investigation are plotted as a function of the pH value and of the concentration of the electrolyte solution.

It is obvious from Fig. 3 that for c.p.-titanium and Ti6Al7Nb no influence on the flatband potential of the phosphate concentration at pH = 7.4 can be detected (resulting from experiments with phosphate concentration diminished by a factor of 10). For the alloy Ti6Al4V the scattering of the flatband potential does not allow valid statements concerning this phenomenon.

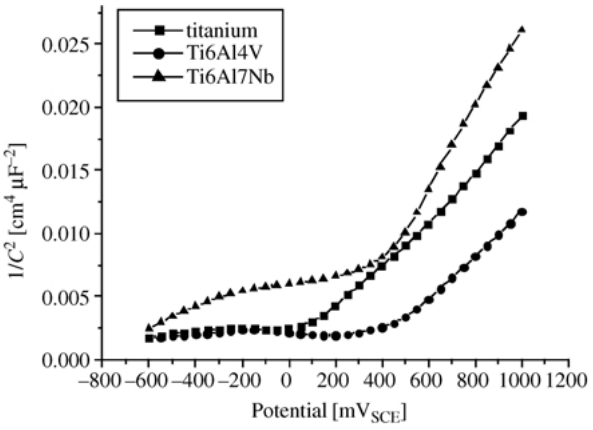

Figure 2 Mott–Schottky plots for air-formed passive layers on c.p.-titanium, Ti6Al4V, and Ti6Al7Nb in 0.133 M phosphate buffer electrolyte pH = 7.4.

TABLE I Flatband potentials and defect densities of c.p. titanium, Ti6Al4V, and Ti6Al7Nb in phosphate buffer solutions of varying pH and concentrations

	Electrolyte	c.p.-titanium	Ti6Al4V	Ti6Al7Nb
U_{FB} [mV_{SCE}]	0.133 M pH = 4.4	66 ± 17	477 ± 74	346 ± 14
	0.133 M pH = 7.4	− 44 ± 21	296 ± 12	165 ± 24
	0.0133 M pH = 7.4	− 64 ± 11	413 ± 67	172 ± 57
	0.133 M pH = 9.2	− 222 ± 32	280 ± 49	− 5 ± 21
N_d [cm^{-3}]	0.133 M pH = 4.4	$(1.52 \pm 0.08) \times 10^{20}$	$(1.85 \pm 0.27) \times 10^{20}$	$(7.78 \pm 0.16) \times 10^{19}$
	0.133 M pH = 7.4	$(1.48 \pm 0.06) \times 10^{20}$	$(1.58 \pm 0.04) \times 10^{20}$	$(8.64 \pm 0.28) \times 10^{19}$
	0.0133 M pH = 7.4	$(1.32 \pm 0.04) \times 10^{20}$	$(1.15 \pm 0.07) \times 10^{20}$	$(7.99 \pm 0.57) \times 10^{19}$
	0.133 M pH = 9.2	$(1.62 \pm 0.12) \times 10^{20}$	$(1.58 \pm 0.03) \times 10^{20}$	$(9.78 \pm 1.07) \times 10^{19}$

In general the flatband potentials of all materials under investigation become more negative with increasing pH-value of the electrolyte solution. But only the graphs of the alloys Ti6Al4V and Ti6Al7Nb in the pH-region between 4.4 und 7.4 give a slope of − 60 mV/pH which is expected from the theory [10]. The slopes for c.p.-titanium are − 99 and − 37 mV/pH in the pH-regions higher and lower than 7.4, respectively. For both alloys slopes of − 9 mV/pH (Ti6Al4V) and − 94 mV/pH (Ti6Al7Nb) were found in the pH-region between 7.4 and 9.2.

Donor densities of the air-formed passive layers have been calculated for all materials from the slopes of the straight parts of the Mott-Schottke plots anodic from the flatband potential according to Fig. 2 for all electrolyte conditions with the assumption of a unified relative dielectric constant of 50 (in analogy to Pan *et al*. [9]). The values are plotted in Fig. 4 versus the pH of the electrolytes similar to Fig. 3. In general no distinct dependence for N_d on the pH can be shown. All donor densities for the materials c.p.-titanium and TiAl6V4 are in the range of $1.5 \times 10^{20}\,cm^{-3}$ and do not significantly differ from each other. The values for Ti6Al7Nb are remarkably lower with around $8 \times 10^{19}\,cm^{-3}$, reaching only about 50% of the others. Table I summarizes the values of U_{FB} and N_d of all investigated materials as a function of the electrolyte conditions.

3.2. Formation of anodic oxide layers by galvanostatic polarization

Figs. 5 and 6 give potential–charge density plots for galvanostatic formation of anodic oxide layers for different current densities and of all materials. The straight lines for the Faraday efficiency ε of the oxide formation with a slope of $2.5\,mC\,V^{-1}\,cm^{-2}$ are based on results by Dyer and Leach [11] as well as own investigations with high current densities, where ε can be assumed to be 100% (data not shown). Under the given experimental conditions a Faraday efficiency below 100% can be attributed only to oxygen evolution as an anodic parallel reaction. This oxygen evolution has a charge transfer by electrons through the anodic oxide layer as a absolutely prerequisite, occurs according to

$$6\ H_2O \rightarrow O_2 + 4\ H_3O^+ + 4\ e^- \qquad (2)$$

and has been proven to take place with a Clark cell experiment (data not shown).

The slopes of the potential–charge density graphs as a measure for the Faraday efficiency of the oxide formation in Fig. 5 show only slight differences for the current density of $6.37\,mA\,cm^{-2}$ with a sequence of Ti6Al7Nb > c.p.-Titan > Ti6Al4V. For the lower current density of $1.27 mA\,cm^{-2}$ in Fig. 6 distinct differences appear between Ti6Al7Nb and c.p. titanium/Ti6Al4V. For the two materials mentioned last a Faraday efficiency close to zero is observed already at potentials $< 10\,V_{SCE}$, which means that the whole charge passed through the system consists nearly completely of electrons transferred through the oxide and consumed by reaction (2).

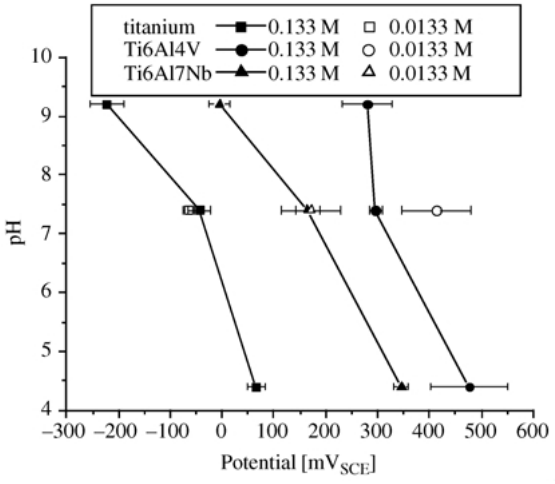

Figure 3 Flatband potentials of air-formed passive layers on c.p.-titanium, Ti6Al4V, and Ti6Al7Nb as function of pH and concentration of phosphate buffer electrolyte.

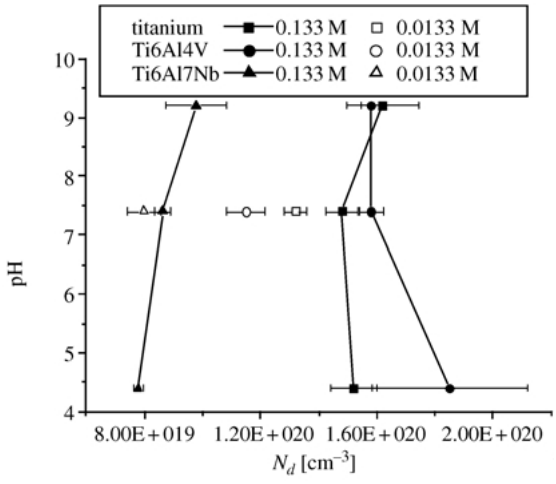

Figure 4 Defect densities of air-formed passive layers on c.p.-titanium, Ti6Al4V, and Ti6Al7Nb as function of pH and concentration of phosphate buffer electrolyte.

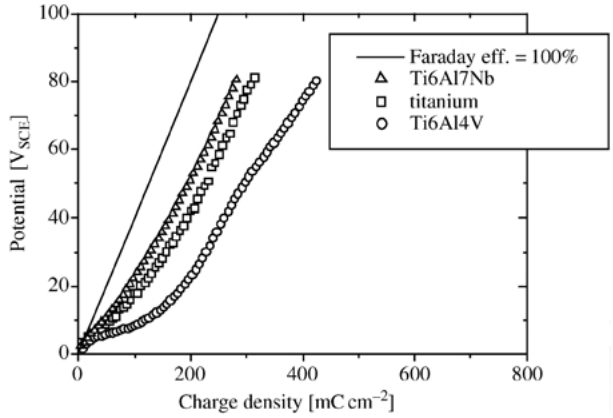

Figure 5 Potential–charge density plots of anodic oxide formation with $i = 6.37\,\mathrm{mA\,cm^{-2}}$ on c.p.-titanium, Ti6Al4V, and Ti6Al7Nb: Faraday efficiency $\varepsilon = 100\%$ corresponds to $2.5\,\mathrm{mC\,V^{-1}\,cm^{-2}}$.

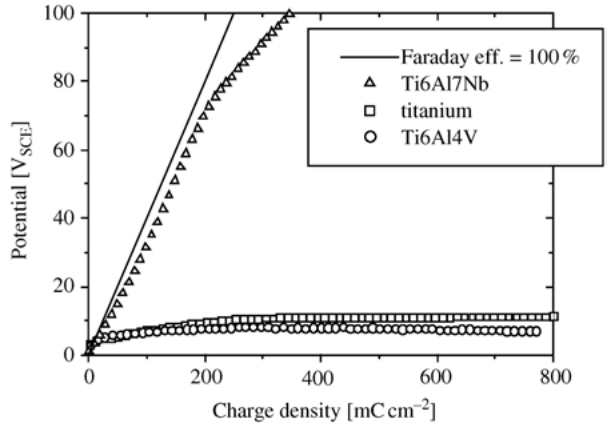

Figure 6 Potential–charge density plots of anodic oxide formation with $i = 1.27\,\mathrm{mA\,cm^{-2}}$ on c.p.-titanium, Ti6Al4V, and Ti6Al7Nb: Faraday efficiency $\varepsilon = 100\%$ corresponds to $2.5\,\mathrm{mC\,V^{-1}\,cm^{-2}}$.

3.3. Scanning electron microscopic investigations of anodic oxide layers

SEM investigations of anodic oxide layers with a formation voltage of $80\,V_{SCE}$ and a current density of $6.37\,\mathrm{mA\,cm^{-2}}$ for all materials investigated are shown in Figs. 7–9. In general a surface morphology containing a blister-like structure that is accompanied by a porosity of the outer part of the oxide layers can be observed for all materials. It is obvious that the number of blisters is much higher on the materials c.p.-titanium and Ti6Al4V than on the alloy Ti6Al7Nb. Fig. 10 visualizes position and origin depth of blisters for an anodic oxide layer on Ti6Al4V polarized with $6.37\,\mathrm{mA\,cm^{-2}}$ up to $80\,V_{SCE}$ in a FIB cross preparation. Apparently the blisters originate almost completely at a distinct depth of about 40% of the total thickness of the oxide layer.

4. Discussion

The flatband potential of a semiconductor electrode corresponds to the point of zero charge (PZC) at the pH-value (and composition) of the given electrolyte solution [10]. The values of U_{FB} in Table I are thus directly related to the isoelectric point (IEP), which can be determined in electrokinetic measurements.

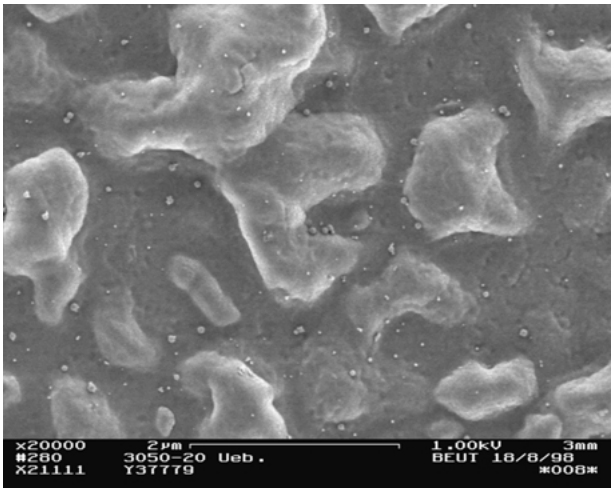

Figure 7 SEM image of surface morphology of anodic oxide layer formed on c.p.-titanium with $i = 6.37\,\mathrm{mA\,cm^{-2}}$ to $U = 80\,V_{SCE}$.

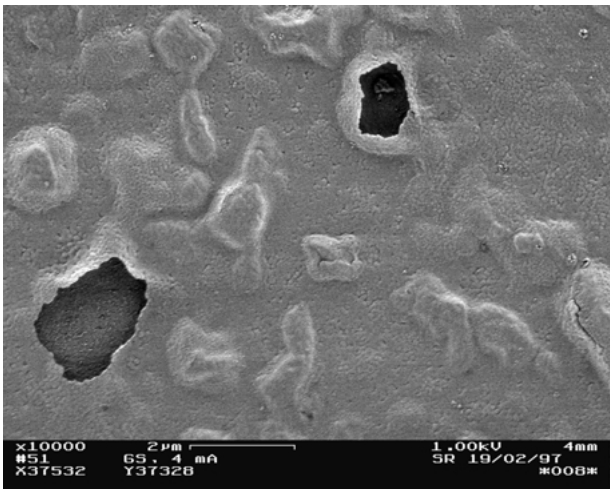

Figure 8 SEM image of surface morphology of anodic oxide layer formed on Ti6Al4V with $i = 6.37\,\mathrm{mA\,cm^{-2}}$ to $U = 80\,V_{SCE}$.

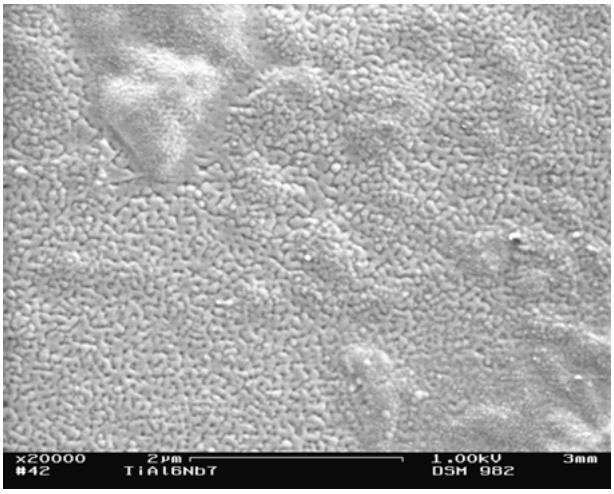

Figure 9 SEM image of surface morphology of anodic oxide layer formed on Ti6Al7Nb with $i = 6.37\,\mathrm{mA\,cm^{-2}}$ to $U = 80\,V_{SCE}$.

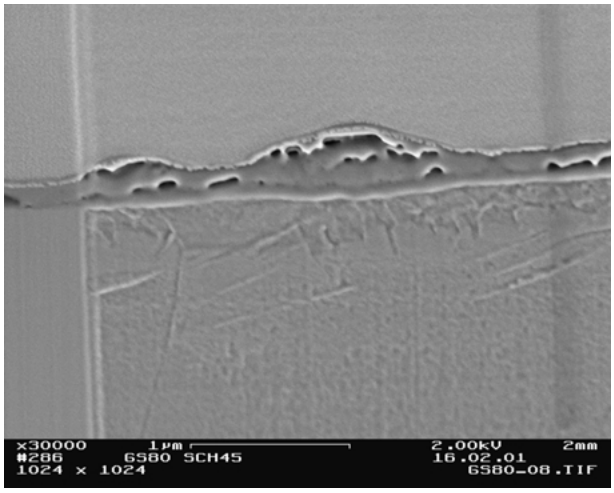

Figure 10 SEM image of anodic oxide layer on Ti6Al4V formed with $i = 6.37\,\mathrm{mA\,cm^{-2}}$ to $U = 80\,\mathrm{V_{SCE}}$: FIB cross section preparation (top, platinum bar; middle, porous oxide layer; bottom, Ti6Al4V substrate).

Corresponding IEP-values have been determined by Rößler *et al*. [12] for c.p.-titanium and Ti6Al4V in KCl-electrolytes of varying concentrations for both air-formed passive layers and in the case of Ti6Al4V additionally anodic oxide layers produced in phosphate buffer pH = 7.4. For all systems comparatively similar IEP-values of 4.5 ± 0.1 (c.p.-titanium) and 4.3 ± 0.1 (Ti6Al4V) were measured.

The results of our investigations cannot be compared directly with that of Rößler *et al*. [12] for two main reasons. One is based on the possible differences between the PZC and the IEP due to specific adsorption of ions which was not excluded completely for chloride by Rößler *et al*. The second reason follows from the variability of the open circuit potential that could not be determined in the investigations of Rößler *et al*. as a function of the pH value and the composition of the electrolyte in the electrokinetic measurements due to limitations of the experimental equipment.

It is discussed in the literature that the open circuit potential of metallic biomaterials *in vivo* is determined by the normal redox potential of biological systems (350–$550\,\mathrm{mV_{SCE}}$) [13]. That means that the *in vivo* status of metallic biomaterials is given by a potential and the pH value of the 'electrolyte'. From that follows that the PZC derived from the flatband potential (characterized by a pH value and the potential) is much better comparable to the situation *in vivo*.

Considering the absolute values of the flatband potentials as well as their pH-dependence for investigated titanium-based materials in Fig. 3 shows that flatband potentials in the region of the *in vivo* redox potential occur only for the both alloys and at pH values below the physiological one. For Ti6Al7Nb a flatband potential of $350\,\mathrm{mV_{SCE}}$ occurs at a pH of about 4.2, for Ti6Al4V at a pH of about 6.5.

For semiconductor electrodes the difference between the open circuit potential (of a oxide covered implant) and the flatband potential of that oxide describes the extent of band bending (conduction band and valence band) in the oxide close to the surface [10]. This extent of band bending gives a measure for the concentration of mobile charge carriers. For n-type semiconductors the concentration of electrons is diminished for $U > U_{FB}$. Thus the difference between the open circuit potential and the flatband potential gives a measure for the rate of charge transfer processes by electrons. From Fig. 3 it follows that this rate should increase in the order Ti6Al4V > Ti6Al7Nb > > c.p.-titanium.

In literature the flatband potential for the system titanium/anodic oxide layer has been systematically investigated predominantly in acid solutions until now. Torresi *et al*. [14] produced oxide layers in 0.5 M sulphuric acid with potentials up to $45\,\mathrm{V_{SCE}}$ and determined the U_{FB} of these layers to be $-540\,\mathrm{mV_{SCE}}$. The U_{FB} was found to be mostly independent from the polarization rate ($5\,\mathrm{mV\,s^{-1}} - 9\,\mathrm{V\,s^{-1}}$). Kudelka *et al*. [15] applied varying oxide formation potentials (1.8–$9.8\,\mathrm{V_{SCE}}$) at titanium grains of different orientation with a polarization rate of $20\,\mathrm{mV\,s^{-1}}$ in the same electrolyte like Torresi *et al*. For titanium grains of different orientation they determined the flatband potentials to be in the range of -350 and $-100\,\mathrm{mV_{SCE}}$. Ohtsuka and Otsuki [16] determined the flatband potential in 0.1 M sulfuric acid and pointed out that the values become more negative with increasing polarization rate ($+20\,\mathrm{mV_{SCE}}$ at $5\,\mathrm{mV\,s^{-1}}$ and $-850\,\mathrm{mV_{SCE}}$ at $500\,\mathrm{mV\,s^{-1}}$). These investigations show clearly that the flatband potential is a sensitive marker for the oxide properties and influenced markedly by the preparation conditions of the oxide layers. As a consequence, it is essential for comparative investigations with different materials to use identical substrate preparation procedures as has been done in this work.

In the case of the formation of anodic oxide layers, that is, for potentials far anodic from the flatband potential, the electronic conductivity of the resulting oxide layer is determined decisively by the donor density. In this context Blackwood and Peter [17] generated anodic oxide layers on titanium in 3 M sulphuric acid using polarization rates between $1\,\mathrm{mV\,s^{-1}}$ and $1\,\mathrm{V\,s^{-1}}$. These investigations indicated that the photocurrent decreases with increasing polarization rate as a function of the potential by 5–30%. The donor density decreases concomitantly by one order of magnitude from 50×10^{19} to $5 \times 10^{19}\,\mathrm{cm^{-3}}$. Investigations of Ohtsuka and Otsuki [16] with anodic oxide layers on titanium in 0.1 M sulphuric acid confirm this results. The donor density is inversely proportional to the logarithm of the polarization rate and decreases between $1\,\mathrm{mV\,s^{-1}}$ and $1\,\mathrm{V\,s^{-1}}$ from about 33×10^{19} to $9 \times 10^{19}\,\mathrm{cm^{-3}}$.

Apart from the influence of the polarization rate, spatially resolved investigations of Kudelka *et al*. [15] showed a correlation between the grain orientation in the metal, the oxide thickness at a given potential, the donor density, and the Faraday efficiency of the oxide formation for potentials $> 4\,\mathrm{V_{SCE}}$ for polycrystalline titanium in 1 N sulphuric acid. In this study $\langle 0\,0\,0\,1 \rangle$ orientations in the metal correspond with thinner oxide layers, higher donor densities, and lower Faraday efficiencies of the oxide formation compared to $\langle x\,x\,x\,0 \rangle$-oriented metal grains.

The literature discussed above indicates, that the influence of the current density on the Faraday efficiency of the oxide formation (difference between Figs. 5 and 6) is in analogy to the influence of the

polarization rate and determined by the donor density in the forming oxide layers which may be influenced by the grain orientation.

Additionally the differences in the behavior of Ti6Al7Nb and c.p.-titanium/Ti6Al4V in Fig. 6 can be explained by the differences in the donor densities of the air-formed passive layers that are the origin for the formation of the anodic oxide layers.

Furthermore, the oxygen evolution as the anodic parallel reaction offers an explanation for the formation of blisters that originate at a distinct depth within the oxide layers. It seems evident that the depth of the formation of oxygen in the oxide layer is bound to a sufficient electronic conductivity of the underlying part of the oxide layer.

For interpretation of the depth of blister formation/oxygen evolution in the anodically formed oxide layers the transfer numbers of titanium and oxygen ions in passive layers ($t_{Ti^{4+}}, t_{O_2^-}$) have to be considered first. Khalil and Leach [18] measured those numbers for different current densities ($6/50\,mA\,cm^{-2}$) with $t_{Ti^{4+}} = 0.35/0.39$ and $t_{O_2^-} = 0.65/0.61$. Based on that a two layer character is generally accepted for the formation of anodic oxide layers in neutral electrolytes [7, 9]. This is explained by simultaneous oxide growth at the phase boundaries metal/oxide and oxide/electrolyte, to an extent that is determined by the transfer numbers $t_{Ti^{4+}}$ and $t_{O_2^-}$. This two layer character should result in an inner phase boundary between that oxide formed due to the transport of oxygen ions and that formed due to the transport of titanium ions. Formation mechanisms should follow solid state reactions (phase boundary metal/oxide) and dissolution-precipitation reactions (phase boundary oxide/electrolyte).

Combining the results from the SEM investigations (Fig. 10) and the aspects discussed above it is obvious that the depth of the origin of the blisters in the cross section of the oxide layer in Fig. 10 is generally identical with the inner phase boundary formed by the two parts of the oxide layers, resulting from different formation mechanisms.

Comparing the different morphology (blister density) of the anodic oxide layers on the investigated materials the distinct differences between c.p. titanium/Ti6Al4V and Ti6Al7Nb correlate well with the different donor densities in the air formed passive layers of those materials. This indicates that the donor densities in the inner part of the anodic oxide layers correlate to those of the air-formed passive layers on the same materials. As a consequence the formation mechanisms of the inner part of the anodic oxide layers and of air formed passive layers seem to be similar in general.

5. Conclusions

Distinct differences in the physico-chemical properties of air formed passive layers and anodic oxide layers formed in neutral electrolytes on c.p.-titanium, Ti6Al4V, and Ti6Al7Nb could be demonstrated by electrochemical and morphological investigations.

These findings offer additional aspects for the explanation of the good biocompatibility of Ti6Al7Nb and suggest that conduction mechanisms, both in air-formed passive layers and anodic oxide layers, contribute significantly to processes that determine the biocompatibility of these materials. In the case of an inflammatory response to an implant with an associated decrease of the pH-value in the surrounding tissue, a significant increase in the electronic conductivity of the passive layer is expected. This is especially true for Ti6Al4V, and may have consequences for possible redox reactions with adsorbed biomolecules. Ti6Al7Nb shows favorable conditions related to low electronic conductivity of the oxide due to the low donor density under physiological conditions and especially in case of anodic oxide layers.

Acknowledgments

Ti6Al7Nb was kindly provided by Dr F. Schlottig, Stratec Medical. Sebastian Tschöcke, TU Dresden, and Dr Horst Wendrock, IFW Dresden, are gratefully acknowledged for EIS-measurements and FIB-preparation, respectively.

References

1. T. HANAWA, K. ASAMI and K. ASAOKA, *J. Biomed. Mater. Res.* **40** (1998) 530.
2. V. KILPADI, G. N. RAIKAR, J. LIU, J. E. LEMONS, Y. VOHRA and J. C. GREGORY, *ibid.* **40** (1998) 646.
3. M. TEXTOR, C. SITTIG, V. FRAUCHINGER, S. TOSATTI and D. M. BRUNETTE, in ''Titanium in Medicine'' (Springer, Berlin, Heidelberg, 2001) p. 171.
4. G. NOGAMI, S. OHKUBO, L. AVALLE and K. HONGO, *J. Electrochem. Soc.* **143** (1996) 3600.
5. S. PIAZZA, L. CALA, C. SUNSERI and F. DI QUARTO, *Ber. Bunsenges. Phys. Chem.* **101** (1997) 932.
6. R. THULL, in ''Metals as Biomaterials'' (John Wiley, New York, 1998) p. 289.
7. D. SCHARNWEBER, in ''Metals as Biomaterials'' (John Wiley, New York, 1998) p. 101.
8. B. A. BOUKAMP, Equivalent Circuit, Version 4.51, University of Twente, 1993.
9. J. PAN, C. LEYGRAF, D. THIERRY and A. M. EKTESSABI, *J. Biomed. Mater. Res.* **35** (1997) 309.
10. H. GERISCHER, *Electrochim. Acta* **35** (1990) 1677.
11. C. K. DYER and J. S. L. LEACH, *J. Electrochem. Soc.* **125** (1978) 1032.
12. S. RÖßLER, R. ZIMMERMANN, D. SCHARNWEBER, H. WORCH and C. WERNER, *Colloids and Surfaces B: Biointerfaces* **26** (2002) 387.
13. D. VELTEN, V. BIEHL, F. AUBERTIN, B. VALESKE, W. POSSART and J. BREME, *J. Biomed. Mater. Res.* **59** (2002) 18.
14. R. M. TORRESI, O. R. CAMARA, C. P. DE PAULI and M. C. GIORDANO, *Electrochim. Acta* **32** (1987) 1291.
15. S. KUDELKA, A. MICHAELIS and J. W. SCHULTZE, *Ber. Bunsenges. Phys. Chem.* **99** (1995) 1020.
16. T. OHTSUKA and T. OTSUKI, *Corr. Sci.* **40** (1998) 951.
17. D. J. BLACKWOOD and L. M. PETER, *Electrochim. Acta* **34** (1989) 1505.
18. N. KHALIL and J. S. L. LEACH, *ibid.* **31** (1986) 1279.

Received 24 May
and accepted 29 May 2002